Materials Research. 2017; 20(3): 786-790
DOI: http://dx.doi.org/10.1590/1980-5373-MR-2016-0824

Nitrogen Oxide (NO) Gas-Sensing Properties of Bi_2MoO_6 Nanosheets Synthesized by a Hydrothermal Method

Ping Tao[a], Yuanlu Xu[a], Yichen Zhou[a], Chengwen Song[a]*, Yinghua Qiu[b], Wei Dong[a], Meihan Zhang[a], Mihua Shao[a]

[a] *College of Environmental Science and Engineering, Dalian Maritime University, 1 Linghai Road, 116026, Dalian, China*
[b] *School of Materials Science and Engineering, Dalian University of Technology, 2 Linggong Road, 116024, Dalian, China*

Received: November 5, 2016; Revised: February 15, 2017; Accepted: April 5, 2017

Bi_2MoO_6 nanosheets were synthesized by a hydrothermal method. Morphology and structure of the Bi_2MoO_6 nanosheets were analyzed by SEM, XRD, N_2 adsorption techniques and XPS. Gas-sensing properties of the as-prepared Bi_2MoO_6 sensors were also systematically investigated. The results showed the reaction temperature greatly affected the morphology and structure of as-prepared Bi_2MoO_6 nanosheets. When the reaction temperature reached 170 ºC, the morphology of the Bi_2MoO_6 nanosheets tended to regular, and pure Bi_2MoO_6 nanosheets were obtained. The operating temperature determined the gas-sensing properties of the Bi_2MoO_6 sensor. At this optimal operating temperature of 300 ºC, the sensitivity of the Bi_2MoO_6 sensor towards 20 ppm nitrogen oxide (NO) reached a maximum of 3.13. With the increase of the nitrogen oxide (NO) concentration, the sensitivity of the Bi_2MoO_6 sensor also rapidly increased, and displayed an almost linear relationship between them. Additionally, the Bi_2MoO_6 sensor demonstrated excellent selectivity with respect to several typical interfering gases.

Keywords: *Preparation, Bi_2MoO_6, Nitrogen oxide (NO), Gas-sensing*

1. Introduction

In the last several years, with the increasing concerns about public safety and human health, there are great demands on precise detection and early warning for environmentally hazardous gases such as NO, NO_2, N_2O, NH_3, H_2S, SO_2, CO, CO_2, and CH_4.[1] Among them, nitrogen oxide (NO) is a typical hazardous gas produced from combustion chemical plants and automobiles, and can cause acid rains, photochemical smog and production of ozone.[2] Therefore, the fast and real-time detection for nitrogen oxide (NO) is very crucial to reduce its harmful effect to environmental and human beings. Currently, traditional detection technologies including optical spectroscopy and gas chromatography usually employ expensive, bulky instruments and complicated sample preparation processes. Therefore, developing miniaturized smart sensors for fast and real-time detection is attracting a great deal of interest.[3] As we know, several kinds of gas sensors have been explored according to different sensing materials and various transduction platforms.[4] Chemiresistive gas sensors based on metal oxides are the most potential candidates because of their advantageous features such as low cost, fast response/recovery time and high compatibility with microelectronic processing.[5-9]

Recently, with the fast development of nanotechnology, a large number of nanostructured materials including SnO_2, WO_3, ZnO, Co_3O_4, and La_2O_3 have been employed for gas-sensing applications.[10] However, compared to these simple binary oxides, multicomponent oxides have greater advantages. For example, they have more freedom to tune the chemical and physical properties of nanomaterials by altering their compositions, which make them more suitable to be adopted as gas sensors.[11] Bi_2MoO_6 is a typical multicomponent metal oxide with a band gap of approximately 2.66 eV. As one of the most important members in the Aurivillius family constructed by $(Bi_2O_2)^{2+}$ layers sandwiched between $(MoO_4)^{2-}$ slabs, Bi_2MoO_6 has aroused extensive attention owing to its potential applications on ferroelectricity, oxide anion conductivity, and non-linear dielectric.[12, 13]

It is well known that the morphologies of nanomaterials have significant effects on their physical and chemical properties. Hence, more attention has been paid on the synthesis of various Bi_2MoO_6 nanostructures, such as nanoparticles, nanoplates, nanofibers, flower-like, cage-like, and hierarchical nanostructures.[14-21]These previous studies reveal that the exploration of Bi_2MoO_6 nanomaterials with different morphologies can achieve versatile properties, which can meet a variety of application needs. In the following, we reported the synthesis of Bi_2MoO_6 nanosheets using a simple hydrothermal method, and investigated the morphologies and gas-sensing properties of Bi_2MoO_6 nanosheets at different reaction temperatures. Finally, we evaluated the practicability

* e-mail: chengwensong@dlmu.edu.cn

and potential of the Bi_2MoO_6 sensor on nitrogen oxide (NO) detection. To the best of our knowledge, there was almost no report concerning Bi_2MoO_6 nanomaterials applied as gas sensors for nitrogen oxide (NO) detection.

2. Experimental

2.1. Preparation of Bi_2MoO_6 nanomaterials

0.06 mol of $Bi(NO_3)_3$▪$5H_2O$ and 0.03 mol of Na_2MoO_4▪$2H_2O$ were added to 100 ml deionized water under stirring. Then 3M HCl was added in the mixed solution until the pH of the solution reached 1.0. Then, the mixture was sealed in a 100 mL Teflon-lined autoclave and heated at 140 ºC, 170 ºC and 200 ºC for 20 h, respectively, and then cooled to room temperature. The resulting precipitates were collected by centrifugation and washed three times by deionized water and ethanol to remove possible impurities. After drying at 60 ºC for 10 h, Bi_2MoO_6 nanomaterials were obtained.

2.2. Characterizations

X-ray diffraction (XRD) patterns of Bi_2MoO_6 nanomaterials were recorded using a D/Max-2400 diffractometer (Cu Kα radiation, λ =1.54055Å) in a range of diffraction angle 2θ from 5º to 85º to analyze the diffraction peaks of Bi_2MoO_6 nanomaterials. The morphologies of Bi_2MoO_6 nanomaterials were observed by a scanning electron microscope (SEM) (Philips XL30 FEG). X-ray photoelectron spectroscopy (XPS) of Bi_2MoO_6 nanomaterials was carried out on Thermo SCIENTIFIC ESCALAB 250 spectrometer with a monochromatic Al Ka source. The porous structure of Bi_2MoO_6 nanomaterials was characterized by nitrogen sorption technique (Quantachrome Autosorb-iQ).

2.3. Fabrication and measurement of Bi_2MoO_6 gas sensor

Bi_2MoO_6 nanomaterials were mixed with several drops of ethanol to form a slurry, and then the slurry was brush-coated onto the surfaces of an alumina tube with two Au electrodes and four Pt wires. A Ni–Cr heating wire was inserted into the alumina tube and used as a heater. The alumina tube was then welded onto a pedestal with six probes to obtain the final sensor unit. Gas sensing tests were performed on a WS-30A static gas-sensing system (HanWei Electronics Co., Ltd., Henan, China) using ambient air as the dilute and reference gas. The test gas with a calculated volume was introduced into the test chamber by a microsyringe.[22]

The sensor sensitivity is defined as follows,

$$Sensitivity = \frac{R_a}{R_g} \quad (1)$$

where R_a and R_g are the electrical resistance of the sensor in air and in test gas, respectively.

3. Results and Discussion

3.1. Morphology and structure of Bi_2MoO_6 nanomaterials at different reaction temperatures

Figure 1 provides the representative XRD patterns of the Bi_2MoO_6 nanomaterials synthesized at the three reaction temperatures (140 ºC, 170 ºC, and 200 ºC). As observed, when the reaction temperatures are 140 ºC and 170 ºC, the Bi_2MoO_6 nanomaterials show the diffraction peaks at 2θ values 23.5º, 28.2º, 32.5º, 33.2º, 36.1º, 46.8º, 47.2º, 55.5º, 56.4º and 58.4º, which are assigned to (111), (131), (002), (060), (151), (202), (260), (133), (191) and (262) planes of Bi_2MoO_6 (JCPDS No. 76-2388), suggesting pure Bi_2MoO_6 nanomaterials are obtained.[23] The sharp and strong intensity of XRD peaks at the two reaction temperatures suggest that the samples have better crystallinity. As reaction temperature is increased to 200 ºC, many extra peaks arising from other phases are detected, indicating impurity phase is introduced in the Bi_2MoO_6 nanomaterials. The morphologies of the as-synthesized samples at different reaction temperatures were investigated by SEM (Figure 2). As observed, when the reaction temperature is controlled at 140 ºC, aggregated and irregular nanosheets and nanoparticles are formed. Increasing the reaction temperature to 170 ºC, the morphology of the Bi_2MoO_6 nanomaterials tended to regular nanosheets. When the reaction temperature reaches 200 ºC, the shape of nanosheets grows more regular, and the sizes of these regular nanosheets are rough several hundreds nanometer.

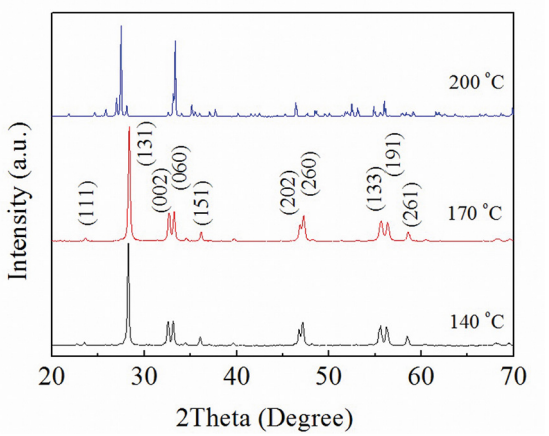

Figure 1. XRD patterns of Bi_2MoO_6 samples.

Figure 3 displays N_2 adsorption-desorption isotherms of the Bi_2MoO_6 samples synthesized at the three reaction temperatures (140 ºC, 170 ºC, and 200 ºC). Obviously, typical IV-type isothermal curves with a hysteresis loop are observed, which implies these materials have mesoporous structure. As measured, the BET specific surface areas of the three Bi_2MoO_6 samples are found to be 16.99 $m^2 \cdot g^{-1}$, 10.43 $m^2 \cdot g^{-1}$, and 8.68 $m^2 \cdot g^{-1}$, respectively, which may result from their different microstructure synthesized at the three temperatures.

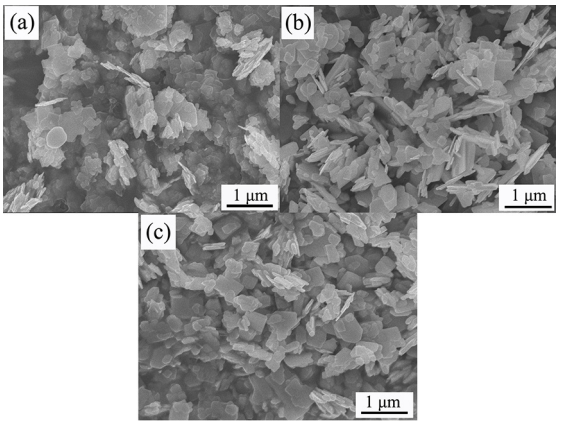

Figure 2. SEM images of Bi_2MoO_6 synthesized at (a) 140 ºC, (b) 170 ºC, and (c) 200 ºC

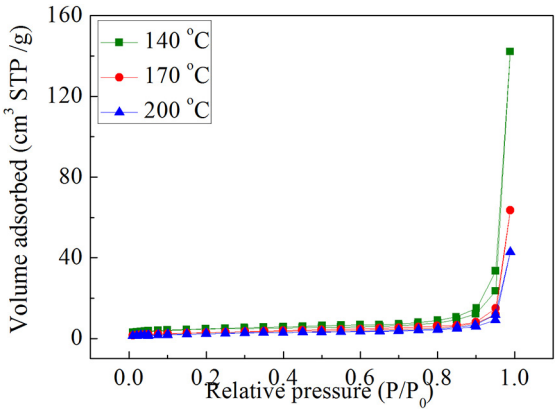

Figure 3. Nitrogen adsorption-desorption isotherms of Bi_2MoO_6 synthesized at (a) 140 ºC, (b) 170 ºC, and (c) 200 ºC.

The chemical composition of the Bi_2MoO_6 nanosheets was analyzed by XPS. The XPS survey spectrum in Figure 4a implies the presence of Bi, Mo and O. Figure 4b-d provide the high-resolution spectra of Bi4f, Mo3d and O1s. The two strong peaks at 159.26 and 164.58 eV belong to $Bi4f_{7/2}$ and $Bi4f_{5/2}$ peaks respectively, revealing the Bi^{3+} oxidation state. The $Mo3d_{5/2}$ and $Mo3d_{3/2}$ peaks located at 232.48 eV and 235.62 eV imply the presence of the Mo^{6+} oxidation state. The XPS spectra of O1s can be deconvoluted into three peaks at 529.75 eV, 530.87 eV, and 531.98 eV, corresponding to the bond of Mo–O, Bi–O, and O–H on the Bi_2MoO_6 nanosheets.[24, 25]

3.2. Gas-sensing properties of Bi_2MoO_6 nanomaterials

The operating temperature has a great influence on the response of the Bi_2MoO_6 sensor towards nitrogen oxide (NO). Figure 5 presents the sensitivity of the Bi_2MoO_6 sensors obtained at 140 ºC, 170 ºC and 200 ºC to 20 ppm nitrogen oxide (NO) as a function of the operating temperature. As observed, the Bi_2MoO_6 sensor synthesized at the reaction temperature of 170 ºC demonstrates high gas sensitivity, which may be ascribed to its regular nonosheet-type structure and high BET specific surface area. The increase in the operating temperature significantly improves the sensitivity of the Bi_2MoO_6 sensor, which reaches a maximum of 3.13 at 300 ºC and then decreases. The phenomenon can be explained by the kinetics and thermodynamics of gas adsorption and desorption on the surface of Bi_2MoO_6 nonosheets. When the operating temperature is lower than 300 ºC, nitrogen oxide

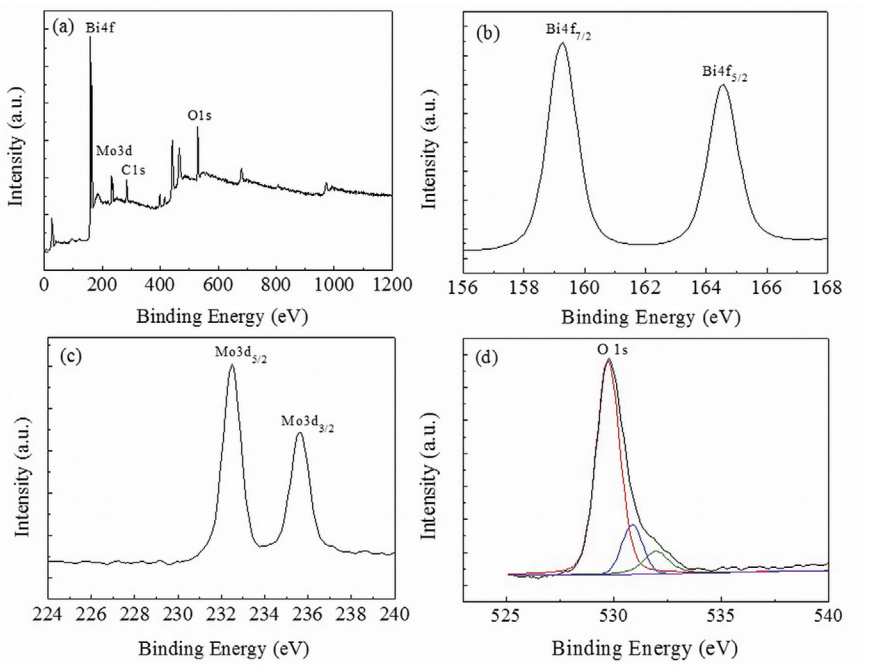

Figure 4. XPS spectra of the Bi_2MoO_6 sample: (a) wide scan spectra, (b) Bi4f spectra, (c) Mo3d spectra, and (d) O1s spectra.

(NO) molecules cannot achieve enough thermal energy to react with adsorbed oxygen species (O_2^-, O^-, O^{2-}), resulting in a low response. On the contrary, when the operating temperature increases beyond a threshold value, the adsorbed oxygen species (O_2^-, O^-, O^{2-}) may escape before reactions, which leads to the decrease of the sensitivity towards nitrogen oxide (NO) as well.[26]

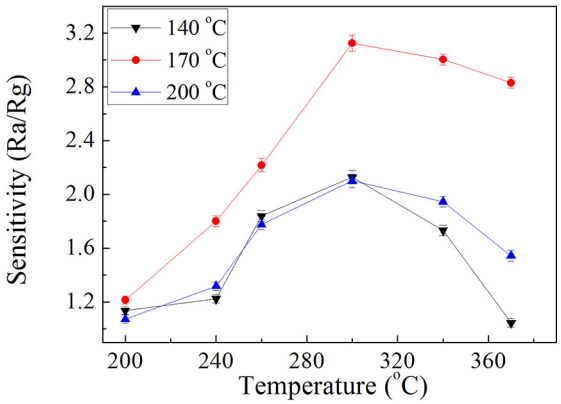

Figure 5. Sensitivity of the Bi_2MoO_6 sensor at different operating temperatures.

Figure 6 provides the relationship between the sensitivity of the Bi_2MoO_6 sensor and nitrogen oxide (NO) concentration (from 10 ppm to 50 ppm). It can be seen that with the increase of the nitrogen oxide (NO) concentration, the sensitivity of the Bi_2MoO_6 sensor also rapidly increases, and displays an almost linear relationship between them, implying the Bi_2MoO_6 sensor is more favorable for detecting low concentration of nitrogen oxide (NO) in real application.[27]

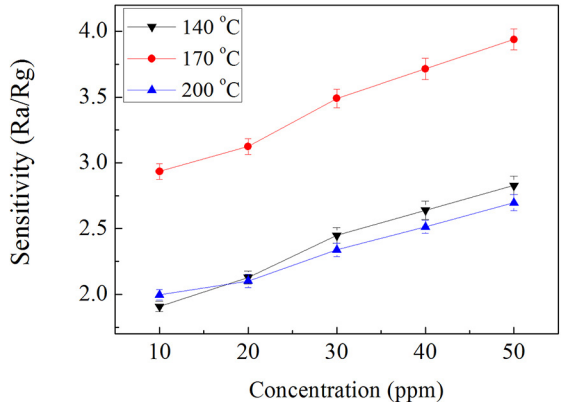

Figure 6. Sensitivity of the Bi_2MoO_6 sensor to different nitrogen oxide (NO) concentrations.

The response of the Bi_2MoO_6 sensor towards nitrogen oxide (NO) can be interpreted by the change in the electrical resistance of the Bi_2MoO_6 sensor, which is usually adopted as a response signal to detect the tested gas. In air, oxygen molecules adsorbed on the surface of the Bi_2MoO_6 sensor will capture electrons from the conduction band and form oxygen species (O_2^-, O^-, O^{2-}), which increases the electrical resistance of the Bi_2MoO_6 sensor. When the Bi_2MoO_6 sensor is exposed to nitrogen oxide (NO), nitrogen oxide (NO) will react with oxygen species (O_2^-, O^-, O^{2-}) and release the trapped electrons back to the conduction band, resulting in the decrease of the electrical resistance of the Bi_2MoO_6 sensor.[28]

In order to investigate the practicability of the Bi_2MoO_6 sensor for nitrogen oxide (NO) detection, the gas-sensing performances of the Bi_2MoO_6 sensor towards other interfering gases were also carried out under the same conditions. Figure 7 presents the nitrogen oxide (NO)-selective characteristics of the Bi_2MoO_6 sensor with respect to several typical interfering gases including CO, CO_2, CH_4, and NH_3. The gas sensitivity of the Bi_2MoO_6 sensor to 100 ppm nitrogen oxide (NO) is 3.94, which is significantly higher than all the other gases. All those indicate that the Bi_2MoO_6 sensor processes excellent selectivity.

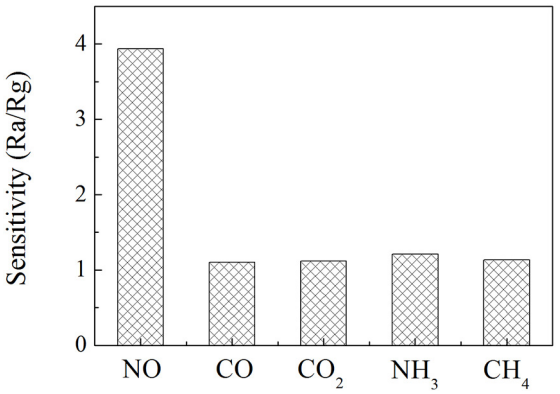

Figure 7. Sensitivity of the Bi_2MoO_6 sensor to other interference gases.

4. Conclusions

We have fabricated the Bi_2MoO_6 nanosheets using a simple hydrothermal method. The XRD and SEM analysis revealed that pure and regular nanosheet-type Bi_2MoO_6 nanomaterials were obtained at the reaction temperature of 170 °C. The XPS wide scan spectra confirmed the presence of Bi, Mo and O in Bi_2MoO_6 nanosheets. The sensitivity of the as-prepared Bi_2MoO_6 sensor towards 20 ppm nitrogen oxide (NO) increased with the increasing operating temperature and then reached a maximum at 300 °C. The Bi_2MoO_6 sensor showed almost linear relationships between the nitrogen oxide (NO) concentration and sensitivity of the Bi_2MoO_6 sensor. In the presence of other interference gases (including CO, CO_2, CH_4, and NH_3), the Bi_2MoO_6 sensor still demonstrated excellent selectivity.

5. Acknowledgement

This work was supported by the National Natural Science Foundation of China (21476034) and the Fundamental Research Funds for the Central Universities (3132016327).

6. References

1. Fan F, Tang P, Wang Y, Feng Y, Chen A, Luo R, et al. Facile synthesis and gas sensing properties of tubular hierarchical ZnO self-assembled by porous nanosheets. *Sensors and Actuators B: Chemical*. 2015;215:231-240.

2. Wetchakun K, Samerjai T, Tamaekong N, Liewhiran C, Siriwong C, Kruefu V, et al. Semiconducting metal oxides as sensors for environmentally hazardous gases. *Sensors and Actuators B: Chemical*. 2011;160(1):580-591.

3. Shi D, Wei L, Wang J, Zhao J, Chen C, Xu D, et al. Solid organic acid tetrafluorohydroquinone functionalized single-walled carbon nanotube chemiresistive sensors for highly sensitive and selective formaldehyde detection. *Sensors and Actuators B: Chemical*. 2013;177:370-375.

4. Llobet E. Gas sensors using carbon nanomaterials: A review. *Sensors and Actuators B: Chemical*. 2013;179:32-45.

5. Ramgir N, Datta N, Kaur M, Kailasaganapathi S, Debnath AK, Aswal DK, et al. Metal oxide nanowires for chemiresistive gas sensors: Issues, challenges and prospects. *Colloids and Surfaces A: Physicochemical and Engineering Aspects*. 2013;439:101-116.

6. Zhang P, Pan G, Zhang B, Zhen J, Sun Y. High sensitivity ethanol gas sensor based on Sn - doped ZnO under visible light irradiation at low temperature. *Materials Research*. 2014;17(4):817-822.

7. Song C, Sun M, Yin Y, Xiao J, Dong W, Li C, et al. Synthesis of Star-Shaped Lead Sulfide (PbS) Nanomaterials and theirs Gas-Sensing Properties. *Materials Research*. 2016;19(6):1351-1355.

8. Corpuz RD, Albia JR. Electrophoretic fabrication of ZnO/ZnO-CuO composite for ammonia gas sensing. *Materials Research*. 2014;17(4):851-856.

9. Yeole B, Sen T, Hansora D, Mishra S. Polypyrrole/Metal Sulphide Hybrid Nanocomposites: Synthesis, Characterization and Room Temperature Gas Sensing Properties. *Materials Research*. 2016;19(5):999-1007.

10. Kolmakov A, Moskovits M. Chemical sensing and catalysis by one-dimensional metal-oxide nanostructures. *Annual Review of Materials Research*. 2004;34:151-180.

11. Lou Z, Deng J, Wang L, Wang L, Zhang T. Curling-like Bi_2WO_6 microdiscs with lamellar structure for enhanced gas-sensing properties. *Sensors and Actuators B: Chemical*. 2013;182:217-222.

12. Li J, Liu X, Sun Z, Pan L. Mesoporous yolk-shell structure Bi_2MoO_6 microspheres with enhanced visible light photocatalytic activity. *Ceramics International*. 2015;41(7):8592-8598.

13. Zheng K, Zhou Y, Gu L, Mo X, Patzkeb GR, Chen G. Humidity sensors based on *Aurivillius* type Bi_2MO_6 (M = W, Mo) oxide films. *Sensors and Actuators B: Chemical*. 2010;148(1):240-246.

14. Martínez-de la Cruz A, Obregón Alfaro S, López Cuéllar E, Ortiz Méndez U. Photocatalytic properties of Bi_2MoO_6 nanoparticles prepared by an amorphous complex precursor. *Catalysis Today*. 2007;129(1-2):194-199.

15. Zhang M, Shao C, Zhang P, Su C, Zhang X, Liang P, et al. Bi_2MoO_6 microtubes: Controlled fabrication by using electrospun polyacrylonitrile microfibers as template and their enhanced visible light photocatalytic activity. *Journal of Hazardous Materials*. 2012;225-226:155-163.

16. López Cuéllar E, Martínez-de la Cruz A, Lozano Rodríguez KH, Ortiz Méndez U. Preparation of γ-Bi_2MoO_6 thin films by thermal evaporation deposition and characterization for photocatalytic applications. *Catalysis Today*. 2011;166(1):140-145.

17. Chen W, Duan GR, Liu TY, Chen SM, Liu XH. Fabrication of Bi_2MoO_6 nanoplates hybridized with g-C_3N_4 nanosheets as highly efficient visible light responsive heterojunction photocatalysts for Rhodamine B degradation. *Materials Science in Semiconductor Processing*. 2015;35:45-54.

18. Wang X, Gu F, Li L, Fang G, Wang X. A facile mixed-solvothermal route to γ-Bi_2MoO_6 nanoflakes and their visible-light-responsive photocatalytic activity. *Materials Research Bulletin*. 2013;48(10):3761-3765.

19. Zhang T, Huang J, Zhou S, Ouyang H, Cao L, Li A. Microwave hydrothermal synthesis and optical properties of flower-like Bi_2MoO_6 crystallites. *Ceramics International*. 2013;39(7):7391-7394.

20. Yin W, Wang W, Sun S. Photocatalytic degradation of phenol over cage-like Bi_2MoO_6 hollow spheres under visible-light irradiation. *Catalysis Communications*. 2010;11(7):647-650.

21. Yan T, Sun M, Liu H, Wu T, Liu X, Yan Q, et al. Fabrication of hierarchical BiOI/Bi_2MoO_6 heterojunction for degradation of bisphenol A and dye under visible light irradiation. *Journal of Alloys and Compounds*. 2015;634:223-231.

22. Tan W, Yu Q, Ruan X, Huang X. Design of SnO_2-based highly sensitive ethanol gas sensor based on quasi molecular-cluster imprinting mechanism. *Sensors and Actuators B: Chemical*. 2015; 212:47-54.

23. Li X, Fang S, Ge L, Han C, Qiu P, Liu W. Synthesis of flower-like Ag/AgCl-Bi_2MoO_6 plasmonic photocatalysts with enhanced visible-light photocatalytic performance. *Applied Catalysis B: Environmental*. 2015;176-177:62-69.

24. Feng Y, Yan X, Liu C, Hong Y, Zhu L, Zhou M, et al. Hydrothermal synthesis of CdS/Bi_2MoO_6 heterojunction photocatalysts with excellent visible-light-driven photocatalytic performance. *Applied Surface Science*. 2015;353:87-94.

25. Zhao J, Lu Q, Wei M, Wang C. Synthesis of one-dimensional α-Fe_2O_3/Bi_2MoO_6 heterostructures by electrospinning process with enhanced photocatalytic activity. *Journal of Alloys and Compounds*. 2015;646:417-424.

26. Wu B, Lin Z, Sheng M, Hou S, Xu J. Visible-light activated ZnO/CdSe heterostructure-based gas sensors with low operating temperature. *Applied Surface Science*. 2016;360(Pt B):652-657.

27. Haija MA, Ayesh AI, Ahmed S, Katsiotis MS. Selective hydrogen gas sensor using $CuFe_2O_4$ nanoparticle based thin film. *Applied Surface Science*. 2016;369:443-447.

28. Chang BY, Wang CY, Lai HF, Wu RJ, Chavali M. Evaluation of Pt/IIn_2O_3–WO_3 nano powder ultra-trace level NO gas sensor. *Journal of the Taiwan Institute of Chemical Engineers*. 2014;45(3):1056-1064.